CASSIA FISTULA GALACTOMANNAN - BASED TERNARY BLEND NOVEL HYDROGEL FOR THE REMOVAL OF MB DYE POLLUTANTS FROM WASTEWATER

Ruchi Singh[a], Jyoti Pandey*[a]

[a] ***Department of Chemistry, B. B. Ambedkar University, Lucknow-226025 (U.P.), India***

Abstract: In the present work, ternary blend hydrogel has been prepared using the thiol modified *Cassia fistula* galactomannan, tragacanth gum, and PEG, cross-linked with glutaraldehyde. The synthesized materials were characterized by using FT-IR, FE-SEM, EDX, XRD and TGA. The ternary blend hydrogel possesses a non-toxic, biodegradable and biocompatible behaviour with low-cost synthesis. The batch adsorption studies of the ternary blend hydrogel were performed, for the removal of toxic cationic dye methylene blue (MB). The adsorption analysis of MB dye was optimized by varying different batch parameters such as pH, adsorbent dose, dye concentration, contact time and temperature. The maximum dye adsorption percentage was achieved up to 93.17 % for methylene blue dye.

Index terms: *Cassia fistula*; tragacanth gum, crosslinking, methylene blue; wastewater

1. INTRODUCTION

Among the current environmental challenges, the most concerning challenge is the waste water treatment which needs a sustainable approach to be cured [1]. Water resources are getting polluted by various toxic contaminations like pesticides, organic impurities, dye effluents and heavy metals [2,3]. These pollutants are continuously being discharged in water resources in a very large amount making the water content unsafe and toxic which causes severe health problems for the public use and other organisms too [4-6]. Industries involved in dyeing, textiles, paper manufacturing, plastics, electroplating and mining often release effluents containing toxic pollutants and heavy metals, which pose serious threats to both human health and the environment. Particularly, dyes and coloring agents, are of significant concern due to their toxic nature and their potential carcinogenic and mutagenic effects. The discharge of these pollutants into water bodies can adversely affect aquatic ecosystems, disrupt environmental balance, and pose substantial risks to public health [7]. Dyes present in industrial effluents are of particular concern, as they can cause various health problems, including allergies, skin irritation and potential carcinogenic effects, even at very low concentrations (e.g., 1ppm). Among these contaminants, methylene blue, a cationic dye, is widely used as a colouring agent in numerous industrial sectors such as textile, pharmaceutical and food-processing industries [8]. Although extensively utilized, the uncontrolled discharge of methylene blue into the environment can pose significant ecological and health risks due to its toxic nature and persistence. Exposure to methylene blue at elevated concentrations may cause adverse

health effects such as skin and eye irritation, dizziness, respiratory discomfort, gastrointestinal disturbance, and other health complications [9-12]. Therefore, the efficient removal of methylene blue from wastewater is essential for protecting both environmental and public health. Water is an essential natural resource that plays a vital role in sustaining life and maintaining ecological balance. However, its quality is increasingly threatened by the discharge of industrial wastes and pollutants into water bodies. To address this issue and ensure the availability of safe and clean water, effective waste water treatment technologies are required. Among the various treatment methods, adsorption has emerged as a simple, efficient, and cost-effective method for the removal of contaminants from wastewater [13,14]. Other conventional treatment methods such as sedimentation, filtration, disinfection and flocculation, have also been employed to mitigate water pollution [15,16]. Nevertheless, these methods, often face limitations in achieving complete purification and may involve higher operational costs.

Consequently, a wide range of adsorbent materials has been developed and investigated for the efficient removal of dyes and other harmful pollutants from aqueous solutions [17-19]. This method is simple to implement and more cost-effective than many other wastewater treatment techniques. However, the synthesis of adsorbents such as polymer-based nanocomposites, biochar, carbon nanotubes, and related materials often involves multistep procedures and harsh reaction conditions such as high temperature and long synthesis time [20,21]. Natural biopolymers exhibit significant potential owing to their biocompatibility, biodegradability, and non-toxicity. They are abundantly available in nature and can be extracted and isolated through relatively simple and low-cost processes. Consequently, these eco-friendly and cost-effective materials have been extensively investigated for addressing a wide range of challenges across various fields. Furthermore, the functionality of biopolymers can be enhanced through chemical modification, which introduces new properties and characteristics without significantly altering their inherent core attributes, thereby expanding their potential applications.

Natural biopolymer-based adsorbents have emerged as promising alternatives for wastewater treatment due to their ease of preparation and environmentally friendly nature. Unlike many synthetic adsorbents, their fabrication generally requires milder processing conditions, shorter preparation times, and lower energy input. In addition, these materials are cost-effective and exhibit excellent adsorption performance toward a wide range of pollutants [20]. Among biopolymer-based adsorbents, hydrogels have gained considerable attention as efficient materials for the removal of dyes and other contaminants from aqueous environments. Their low cost, simple preparation, and high adsorption capacity make them attractive candidates for wastewater remediation applications [19]. Hydrogels are three-dimensional polymeric networks capable of absorbing and retaining large amounts of water or aqueous solutions [7,22,23]. The extent of water uptake is influenced by factors such as polymer composition, network architecture, and the degree of cross-linking [24,25]. The characteristics and performance of hydrogels can be tailored by incorporating specific functional groups into their polymeric network. Various modification techniques, including cross-linking and grafting, are commonly employed to enhance their mechanical strength, adsorption efficiency, and overall functionality for targeted environmental applications [26-28].

Cross-linked hydrogel networks have attracted significant attention owing to their wide range of applications in fields such as biomedicine, agriculture, environmental remediation, and water purification [7, 25, 26]. Among these applications, their use in environmental engineering is particularly important, as hydrogels provide an effective and sustainable approach for the removal of industrial pollutants and other contaminants from water resources [7]. To address water pollution challenges, numerous synthetic and naturally derived hydrogels have been developed [29,30]. However, hydrogels prepared solely from natural polymers often exhibit limited mechanical strength and structural stability, restricting their performance under demanding application conditions. To overcome these limitations, researchers have focused on developing hybrid or blended hydrogels that combine the advantages of both synthetic and natural polymers [27]. Such composite systems offer improved mechanical integrity, enhanced durability, and better functional performance, making them more suitable for large-scale and practical applications. Furthermore, the stability and strength of hydrogel networks can be further enhanced through the use of crosslinking agents. Various chemical cross-linkers, including epichlorohydrin [31], glutaraldehyde [32,33], and genipin [34], have been widely employed to reinforce the polymer matrix and improve the overall physicochemical properties of hydrogels.

Thiolated *Cassia fistula* gum is a chemically engineered polysaccharide derived from *Cassia fistula* seed gum through the introduction of thiol groups onto its polymeric backbone. The presence of these thiol groups significantly improves its water absorption capability, adsorption performance, and network-forming potential by facilitating disulfide bond formation. Owing to these enhanced characteristics, thiolated *Cassia fistula* gum has attracted considerable interest as a sustainable biomaterial for the development of hydrogels and pollutant removal systems [35].

Tragacanth gum is a naturally derived polysaccharide that has gained considerable attention as a sustainable material for the fabrication of eco-friendly hydrogels [36-40]. It is obtained from various species of the Astragalus plant and possesses a highly branched, heterogeneous molecular structure [41]. The presence of abundant hydroxyl and carboxyl functional groups within its polymeric framework allows it to undergo chemical and physical modifications, thereby improving its physicochemical properties and expanding its range of applications [42,43]. Due to its non-toxic nature, low cost, biodegradability, biocompatibility, and stability across a broad pH range, tragacanth gum has emerged as a promising biopolymer for the development of environmentally benign materials [44].

The present study aims to design and synthesize a novel multicomponent green hydrogel based on a biopolymeric matrix and reinforced through cross-linking with a dialdehyde-based cross-linking agent. This research was motivated by the growing environmental concern associated with the discharge of toxic dyes into aquatic ecosystems. To evaluate its potential as an adsorbent, the synthesized hydrogel was tested for the removal of the cationic dye methylene blue from aqueous media. The adsorption performance was systematically investigated by examining the effects of several operational parameters, including initial dye concentration, solution pH, contact time, temperature, and adsorbent dosage. These studies were conducted to assess the efficiency of the hydrogel in removing dye contaminants from wastewater through the adsorption process.

2. NEED OF THE STUDY

This study plays a significant role in environmental remediation by treating polluted water which is a major factor to be considered. The need was to develop an environmental-friendly adsorbent which was prepared by using natural biopolymers leading a low-cost synthesis. Aiming this, we have developed a novel ternary blend that was prepared using biopolymer base and further crosslinking it with a dialdehyde chemical crosslinking agent. The work is done considering a serious environmental issue which is to remove toxic dye pollutants from wastewater systems. The synthesized ternary blend hydrogel was examined against a cationic dye methylene blue and various parameters have been checked to study the removal of dye from aqueous solution via adsorption method. Different parameter tests were performed by varying dye concentration, pH, contact time, temperature and adsorbent dose.

3. EXPERIMENTAL SECTION

3.1 Materials and Methods

3.1.1 *Materials*

The galactomannan was extracted from the seeds of *Cassia fistula* plant. The seeds were collected from the *Cassia fistula* pods from the Babasaheb Bhimrao Ambedkar University campus, Lucknow, 226025, India. The other reagents and solvents were procured from the local suppliers and all the chemicals were utilized without any further purification. The double distilled water was used during all the experimental set-up.

3.1.2 Characterization of modified gum and hydrogel

3.1.2.1 FT-IR Analysis

The synthesized blended Hydrogel and other components were observed under Fourier Transform Infrared Spectroscopy in a FT-IR spectrophotometer of Perkin Elmer Two Spectrophotometer via KBr pellet method in a range of 4000 to 500 cm-1. The powdered samples were pulverized with KBr in a pestle and mortar. The powder was compressed under an IR hydraulic press to form a pellet and the spectra was recorded for the same.

3.1.2.2 Field Emission Scanning Electron Microscopy (FE-SEM) Analysis

The surface analysis and shape of the Hydrogel materials were examined using field emission scanning electron microscope (Nova Nano SEM 450, USA). The powdered materials were mounted on a sample holder followed by a coating of platinum on them. The images were then captured at different resolutions.

3.1.2.3 Energy dispersive X-Ray microanalysis (EDX):

The samples were examined through EDX to confirm the presence of elemental content by using FE-SEM-EDX model Nova Nano SEM 450, USA.

3.1.2.4 X-Ray Diffraction (XRD) Analysis

The X-Ray diffraction studies of the samples were observed by using an X-Ray diffractometer of BRUKER, Germany having model D8 Advance Eco. The study was done to investigate the crystalline or amorphous nature

of the samples. Samples were finely powdered and scanned for a diffraction angle (2Θ) ranging in between 10° to 90°. The conditions of voltage and current for experiment was kept to be 40 KV and 40 mA, respectively.

3.1.2.5 Thermogravimetric Analysis

The thermogravimetric analysis of all samples was recorded using a TGA instrument EXSTAR S11 6300 in nitrogen atmosphere with temperature ranging from 50℃–800℃.

3.1.3 Synthesis

3.1.3.1 Isolation and modification of CF Gum

The biopolymer source was collected from the *Cassia fistula* plant also known as "golden shower" or "amaltas". The seeds were separated from the pods of the plant then washed and dried to make a coarse powder of it. *Cassia fistula* galactomannan was isolated from the coarse seed powder by our research group following a previously reported method [45]. Thiolation of the isolated galactomannan was subsequently carried out via esterification with thioglycolic acid using the procedure described in our earlier work [35].

3.1.3.2 Synthesis of Glu-hydrogel

The multicomponent hydrogel was prepared by adopting the crosslinking methodology. The powdered thiolated *Cassia fistula* (TCF) gum (0.2 g) was suspended in distilled water until homogenizes at 50 ℃ with continuous stirring for 30 min. Separately, tragacanth gum (TG) (1.5 g) and polyethylene glycol (PEG) (0.3 g) were homogenised in distilled water at 50℃ with stirring for 30 min each. After complete homogenization of the materials, modified TCF gum dispersion was mixed with tragacanth gum and stirred for 1 h, followed by the addition of PEG solution. The reaction mixture was stirred for 10 min and then the crosslinking agent glutaraldehyde (1 ml) was added dropwise to this reaction mixture over 5 min and further the gel mixture was formed while stirring continuously for 2 h. The gel mixture was poured in a petri dish and stored in an oven at 50 ℃ till completely dry and reduced to a fine powder. The synthesized hydrogel was examined by FT-IR, FE-SEM, EDS, XRD and TGA thermal analysis.

3.1.3.3 Batch adsorption experiment of dye

The MB dye removal studies were conducted via adsorption method. A 1000 ppm stock solution of MB dye was prepared in 250 ml distilled water. The other experimental solutions were prepared by diluting the stock solution with distilled water till specific concentrations were achieved. Optimization of different parameters were done by batch experiments to check efficiency of dye uptake from aqueous solutions. The initial dye concentrations, solution pH, adsorbent dose, temperature and contact time parameters were varied in a specific range. The equilibrium adsorption concentration was obtained by the initial concentration behaviour against MB dye. The dye adsorption studies were recorded using a Double beam UV spectrophotometer (Cary100). The dye adsorption capacity at equilibrium (Qe) and the percentage removal (% R) of dye was evaluated using eq. 1 and 2, respectively.

$$Q_e = \frac{(C_i - C_e)V}{m} \quad (1)$$

$$\% R = \frac{(C_i - C_e)}{C_i} 100 \quad (2)$$

Here; the terms 'Ci' denotes the initial dye concentration (mg/L), 'Ce' represents the dye concentration at equilibrium (mg/L), 'm' is the mass of adsorbent (g) and 'V' is the total volume of the dye solution (L).

3.1.3.4 Adsorption isotherms

The adsorption isotherms were calculated using the batch study of methylene blue dye concentrations. The adsorption equilibrium data at different initial concentrations of MB dye was noted to fit isotherm models. The isotherm models were selected for explanation of solid-liquid phase adsorption and were fitted in their non-linearized forms. The models included two parameter-based models, three parameter-based models and four parameter-based models. The non-linear equation forms of isotherm models along with their parameter descriptions are given in Table 1a-c.

Table 1a. Two parameter-based adsorption isotherm models and their forms.

Sr. No.	Isotherm models	Parameter explanation	Non-Linear form
1	Langmuir	**q_e** is the dye adsorption capacity; **C_e** is the equilibrium concentration of dye; **q_m** is the maximum adsorption capacity; and **K_L** is the Langmuir constant relating to the binding energy.	$q_e = q_m K_L \frac{C_e}{1 + K_L C_e}$
2	Freundlich	**q_e** is the dye adsorption capacity; **C_e** is the equilibrium concentration of dye; **K_F** is the Freundlich constant; **1/n** is constant denoting the adsorption intensity.	$q_e = K_F {C_e}^{1/n}$
3	Dubinin - Radhuskevich	**q_e** is the adsorption capacity; **C_e** is the equilibrium concentration of dye; **q_m** is the maximum adsorption capacity of dye; **β** is the D-R constant; **ϵ** is the Polanyi potential; **R** is the gas constant; **T** is the reaction temperature.	$q_e = q_m . e^{-\beta\left(RT \ln\left(1+\frac{1}{C_e}\right)\right)^2}$ $\epsilon = RT \ln\left(1 + \frac{1}{C_e}\right)$
4	Temkin	**q_e** is the adsorption capacity; **C_e** is the equilibrium concentration of dye; **K_T** is the Temkin constant; **B** is the constant denoting heat of adsorption.	$q_e = B \ln(K_T C_e)$

5	Jovanovic	**q_e** is the adsorption capacity; **C_e** is the equilibrium concentration of dye; **q_m** is the maximum adsorption capacity of dye; **K_{JV}** is the Jovanovic constant.	$q_e = q_m(1 - e^{-K_{JV}C_e})$

Table 1b. Three parameter-based adsorption isotherm models and their forms.

Sr. No.	Isotherm models	Parameter explanation	Non-Linear form
1	Koble Corrigan	**q_e** is the dye adsorption capacity; **C_e** is the equilibrium concentration of dye; **AC_e^n** represents the Freundlich model; **$1+B\,C_e^n$** represents the Langmuir model. **A, B,** and **n** are the Koble model constants.	$q_e = \frac{AC_e^n}{1 + B.C_e^n}$
2	Redlich-Peterson	**q_e** is the dye adsorption capacity; **C_e** is the equilibrium concentration of dye; **A_{RP}, K_{RP}** is the isotherm model constants; **m** is the model exponent ranging from 0 to 1.	$q_e = \frac{K_{RP}C_e}{1 + A_{RP}.C_e^m}$
3	Liu	**q_e** is the dye adsorption capacity; **q_m** is the maximum adsorption capacity of dye; **C_e** is the equilibrium concentration of dye; **K_{Liu}** Liu model constant relating to the binding energy; **n** is Liu exponent which relates to the surface heterogeneity.	$q_e = \frac{q_m(K_{Liu}C_e)^n}{1 + (K_{Liu}C_e)^n}$
4	Khan	**q_e** is the dye adsorption capacity; **q_m** is the maximum adsorption capacity of dye; **C_e** is the equilibrium concentration of dye; **K_{KH}** is the Khan isotherm constant; **α_{KH}** is the Khan model exponent.	$q_e = \frac{q_m K_{KH} C_e}{(1 + K_{KH}C_e)^{\alpha_{KH}}}$
5	Jossens	**q_e** is the dye adsorption capacity; **C_e** is the equilibrium concentration of dye; **K_J, J_S,** and **a** are the Jossens isotherm constants.	$q_e = \frac{K_J C_e}{1 + J_S C_e^a}$

Table 1c. Four parameter-based adsorption isotherm models and their forms.

Sr. No.	Isotherm models	Parameter explanation	Non-Linear form
1	Fritz Schlunder	**q_e** is the dye adsorption capacity; **C_e** is the equilibrium concentration of dye; **q_m** is the maximum adsorption capacity of dye; **K_1, K_2,** and **m** are the model parameters.	$q_e = \frac{q_m K_1 C_e}{1 + (K_2 C_e^m)}$

3.1.3.5 Adsorption kinetics

The investigation of adsorption kinetic models for MB dye removal from aqueous solution was done on the basis of batch parameter contact time. The contact time was varied in a range from 60 min to 360 minutes. The

kinetic studies in adsorption process offers valuable features involving adsorption mechanisms and its reaction pathways. To study mechanism there are various kinetic models which were drawn to get the best fitted kinetic model with the experimental data. Kinetic models like Pseudo-first order, Pseudo-second order, Elovich, and Intraparticle diffusion were implemented to determine the rate of dye removal process [46].

4. RESULTS AND DISCUSSION

4.1 Synthesis of glutaraldehyde crosslinked ternary blend hydrogel

The blended hydrogel was synthesised by blending natural biopolymer (tragacanth gum and TCF gum) with synthetic polymer (PEG) which was cross-linked with glutaraldehyde following the conditions as shown in Scheme 1.

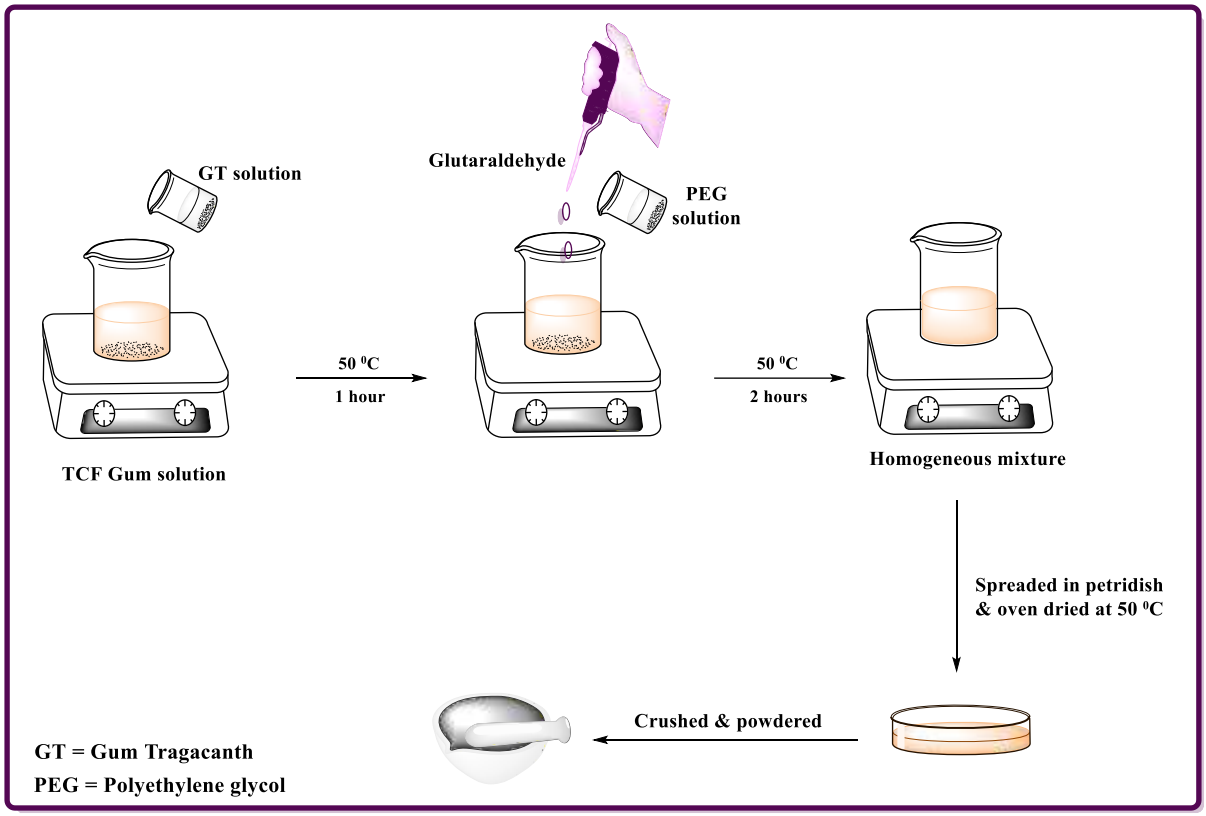

Scheme 1. Synthesis scheme for preparation of Hydrogel.

4.2 Characterization results

4.2.1 FT-IR spectra

FT-IR spectral analysis of all the samples is shown in Figure 1. The spectra of modified TCF gum (─A) showed a characteristic broad peak of ─OH stretching vibration of galactomannan backbone at a region 3100–3650 cm-1, ─CH stretching vibration at 2887 cm-1 [47], the peaks at 1505 cm-1 and 1403 cm-1 attributed due to the ─CH alkane bending vibrations [45, 47, 48]. A band at 2079 cm-1 was obtained which resembles ─SH stretch in thiol modified gum [49]. The FT-IR spectrum of gum tragacanth (─B) shows adsorption band for ─OH stretching vibration in the range of 3100-3700 cm-1. The adsorption bands of carbonyl or carboxylic groups

(C=O, COOH) were observed at 1730 cm-1, the peak at 1643 cm-1 can be attributed due to carboxylic acid or carboxylate anion form of d-galacturonic acid present in tragacanth gum polymer unit. The peaks at 1450 cm-1 and 1352 cm-1 were assigned to C─OH deformation vibration with contribution of C─O─C symmetric stretching vibration of carboxylate group. The peaks at 1250 cm-1 and 1099 cm-1 were related to C─O─C asymmetric stretching vibration in glycosidic groups of polysaccharides [50, 51]. As similar to the spectrum of TCF gum and tragacanth gum, the resembling FT-IR spectra has been obtained for Hydrogel (─C) which shows an overlapping pattern to both the spectrum.

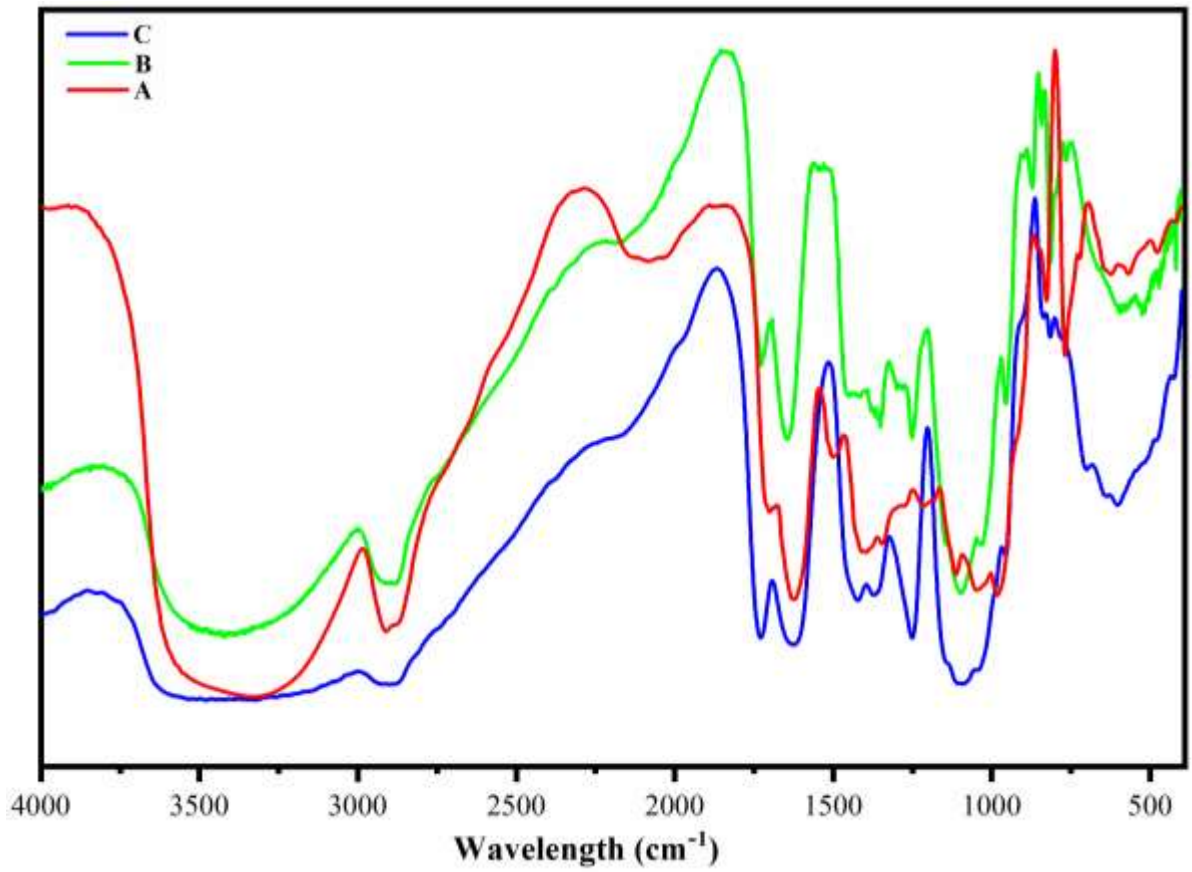

Figure 1. FTIR of TCF gum (─A), Gum Tragacanth (─B) and Hydrogel (─C).

4.2.2 FE-SEM micrographs

Field emission scanning electron microscopic (FE-SEM) images were recorded to analyse the morphological studies of the modified TCF (A1) gum and Hydrogel (B1) as shown in Figure 2. The FE-SEM micrographs indicates the significant difference in morphologies of all the samples. Both the images show roughness at their surface morphologies. The modified TCF gum exhibits surface roughness and shows relatively big particles whereas the blended hydrogel material shows rougher surface relative to the other sample and the particles exhibits close resemblance to the modified TCF gum.

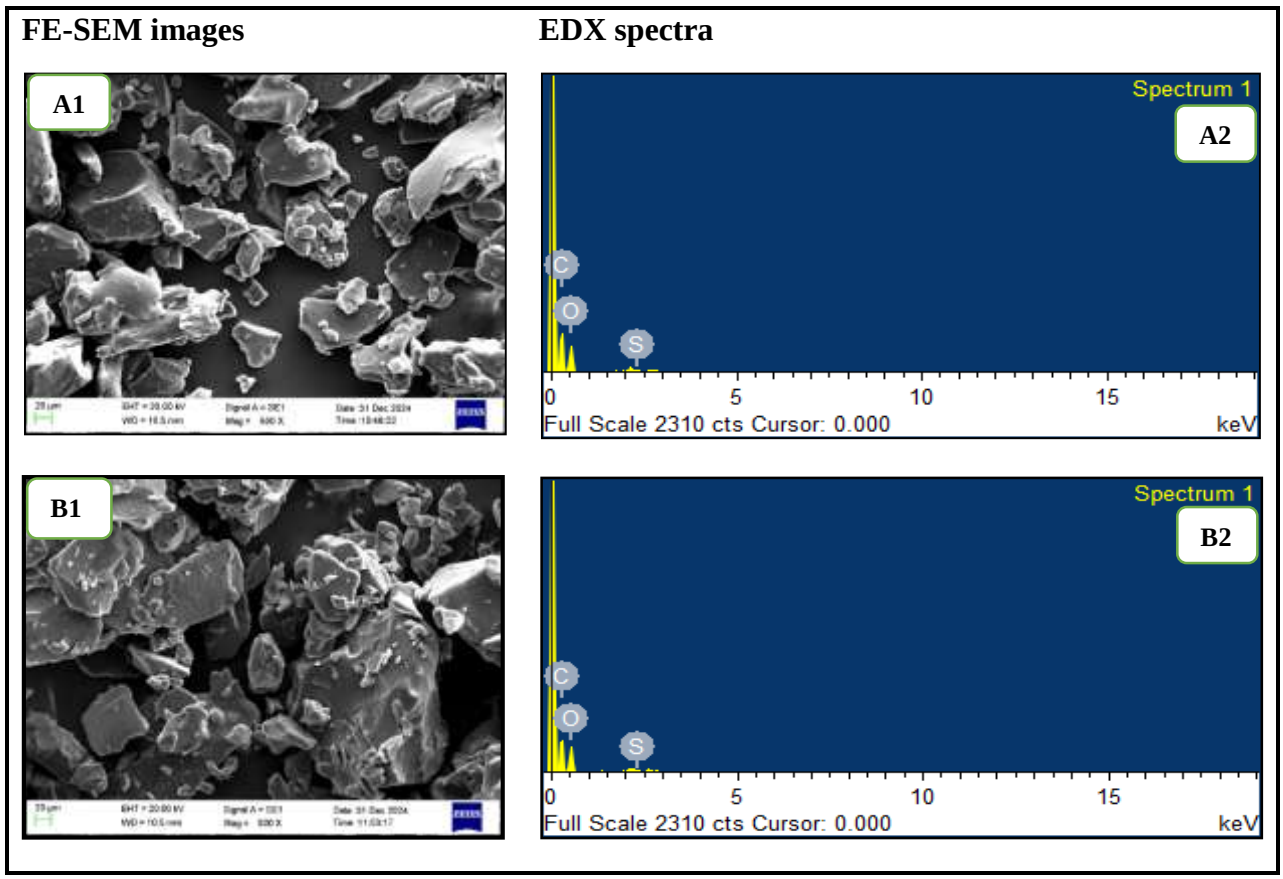

Figure 2. FE-SEM images and EDX spectra of TCF gum (A1, A2) and Hydrogel (B1, B2).

4.2.3 EDX analysis

The EDX analysis of all the materials are given in Figure 2 which shows the presence of carbon, oxygen, sulphur in the both modified TCF gum (A2) moiety as well as in the blended structural composition of hydrogel (B2). This clearly indicates that the synthesis of crosslinked blended hydrogel has been successfully achieved.

The images of elemental mappings for the thiolated galactomannan material and the hydrogel samples are shown in Figure 3. The elemental mapping shows that the images were having a good composition of carbon, oxygen and sulphur inside the polymeric unit which indicates the relative assurance to the EDX spectra of both TCF gum and hydrogel. The presence of elements confirms the successful modification of galactomannan and synthesis of hydrogel matrix.

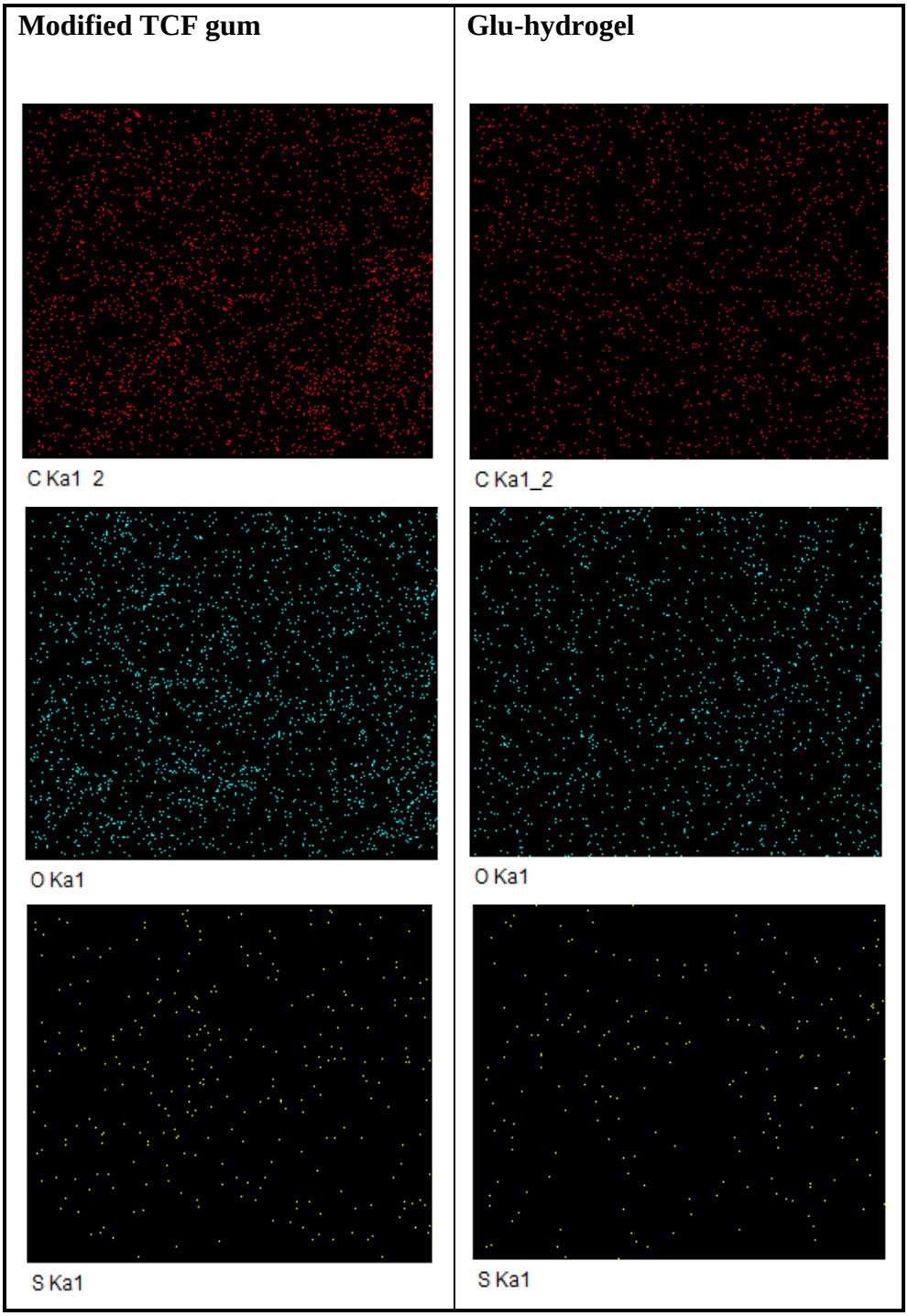

Figure 3. Images for elemental mapping in modified TCF gum and Hydrogel materials.

4.2.4 XRD

The XRD pattern for modified galactomannan and hydrogel samples are represented in Figure 4 which shows broad peaks for 2Θ angle values around 20.17° indicates about the amorphous nature of the TCF modified gum. The XRD results make it clear that both the samples are in amorphous form having a slight noticeable change in 2Θ values. However, the Hydrogel also shows amorphous nature having the 2Θ values around 18.80° and 26.58°.

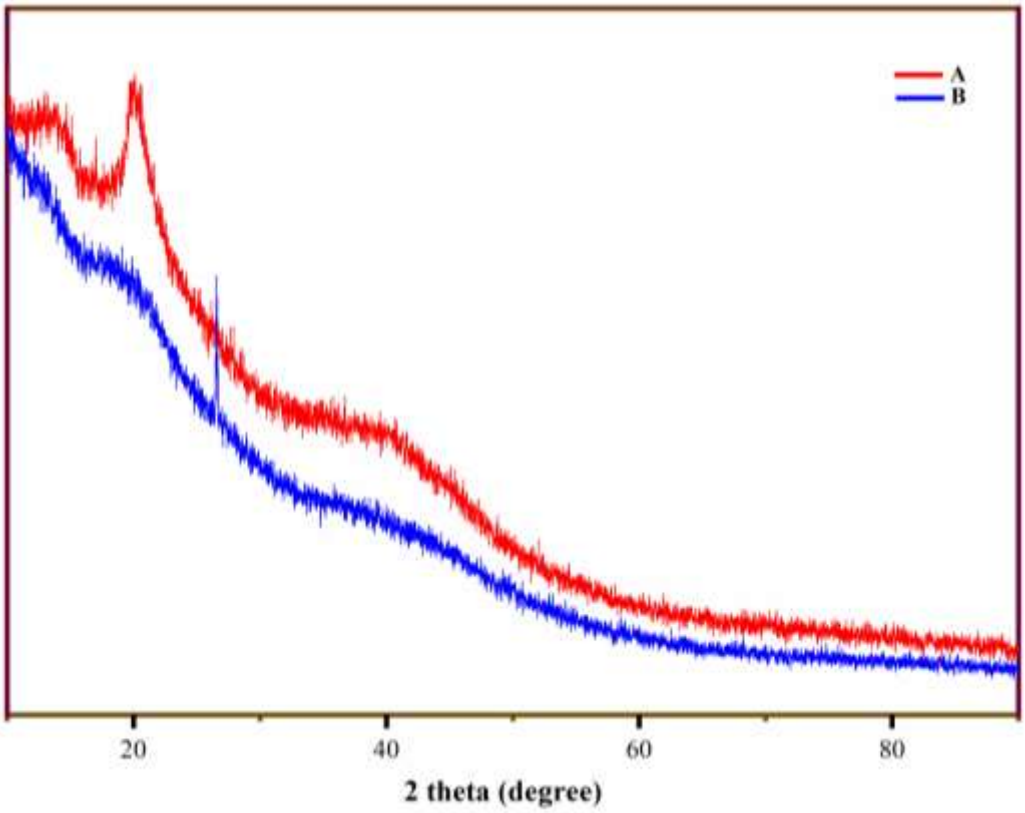

Figure 4. XRD spectrum of TCF gum (─A) and Hydrogel (─B).

4.2.5 TGA analysis

To determine the thermal stabilities of both the materials, the TGA study was performed and the plots for the same are given in Figure 5. The thermal studies of both the samples clarifies that the hydrogel (─B) is comparably thermally stable than the modified TCF gum (─A) and shows a significant weight loss. For thiol modified gum, the first weight loss stage occurs in a temperature range of 80℃–287℃ which may be a reason of evaporation occurred to the bounded and unbounded water molecules. The further weight loss was found around a range of 288℃–800℃ indicating the degradation of the polymer backbone consisting of polysaccharides matrix. The thermal analysis for hydrogel sample shows a percentage weight loss at the first stage ranging around 200℃–250℃ as shown in Figure 5 due to the evaporation of the water molecules and secondly the weight loss has shown around 290℃– 410℃ because of the degradation of polymeric chains in the hydrogel matrix. Both thermogram shows close resemblance after reaching a temperature ranging 500℃–800℃.

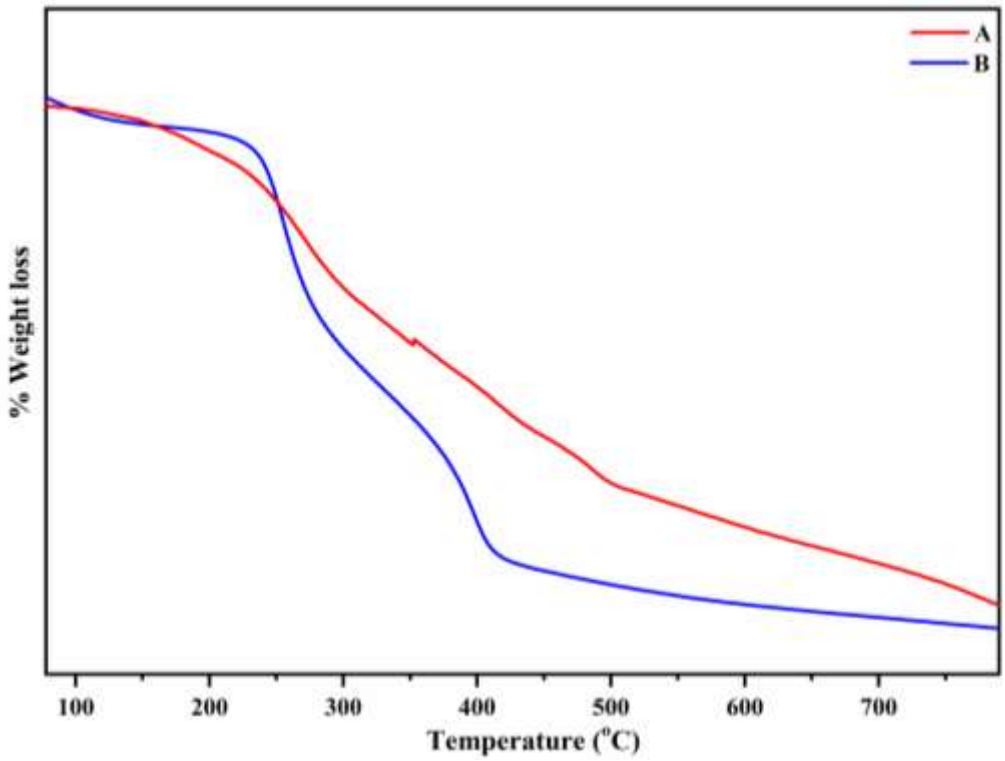

Figure 5. TGA plots of TCF gum (─A) and Hydrogel (─B).

4.3 Effect of batch parameters

4.3.1 Initial concentration of dye

The batch adsorption experiments were performed by altering one parameter at a time. The concentration of methylene blue dye solution was varied in a range 250–550 mg/L. The other parameters (adsorbent dose, volume, contact time and pH) were kept constant. The adsorbent dose was added as 1% w/v to the experimental solutions. The adsorption of methylene blue dye was gradually decreased while increasing the concentration from 250 mg/L to 550 mg/L. This may be due to the increased number of adsorbate molecules interacting electrostatically to the polymer chain [52]. The dye removal trend corresponding to the dye concentration is shown in Figure 6 (A). As the maximum removal 92.74 % of dye has been observed at a concentration 250 mg/L, so this concentration was opted as the initial concentration for further batch parameter studies. This study is considered as one of the important adsorption studies to check the further batch parameters.

4.3.2 Variation of adsorbent dose

The amount of adsorbent dose (Hydrogel) was optimized in a range of 5 mg to 60 mg. All the other parameters like dye concentration, solution volume, temperature, contact time and pH were kept unchanged. Various adsorbent dosage was added to the 250 mg/L dye experimental solutions [53]. The dye removal was first increased and then achieved a constant removal by the increasing adsorbent dosage as shown in Figure 6 (B). This may be due to the active sites for adsorption were increased and achieved a stable adsorption on the high adsorbent dosage. The maximum percentage removal of 93.55 % is shown at dose of 20 mg. This maximum removal dose value was considered as an appropriate adsorbent dose for the other batch parameters.

4.3.3 Effect to contact time

Another important parameter while studying adsorption experiment of any dye is the contact time of the solution to the adsorbent. The samples were tested for a contact time up to 6 hours for the dye solution. The highest percentage dye removal value for Hydrogel against MB dye was observed at 300 min is 93.34 %. The optimization graph of contact time for Hydrogel adsorbent is given in Figure 6 (C). The increased trend of dye removal was observed due to the interactions of active sites of adsorbent were formed better with MB dye molecules during 300 minutes contact time [54].

4.3.4 Effect of pH

The batch adsorption studies were further checked at different pH of the dye solution keeping the other parameter constants (initial conc. = 250 ppm, adsorbent dosage = 20 mg, contact time = 300 minutes, temperature and solution volume). The pH solutions were prepared while adjusting with HCl and NaOH solutions and examined a pH range of ranges from 1 to 11. The effect of pH on dye removal is shown in Figure 6 (D). From graph, it has been clearly seen that the dye removal was firstly increased with increasing pH and after reaching maximum removal it shows a slow decrease in % dye removal. The high percentage dye removal is achieved at a neutral solution pH 7 with a removal value of 93.26 %. The poor dye removal at low pH value of the MB dye was due to either competitive adsorption between the H+ ions and cationic MB+ molecules or H-bonding between the ─COOH group and MB dye molecules. Enhanced dye uptake at neutral pH value was may be because of the ionization and increased electrostatic attractions among the positively charged adsorbate and negatively charged adsorbent molecules [46].

4.3.5 Effect of temperature

After achieving above results, the other parameter was analysed to check the thermal conditional behaviour of adsorbent in the dye solution. The temperature of dye solution was varied and the percentage removal is shown in Figure 6 (E). The graph shows an increasing pattern of dye removal with the increasing value of temperature and then after achieving maximum removal it and then a rapid decrement was found followed by negligible changes at further temperatures making a stable removal trend. The highest dye removal 92.97 % was occurred at temperature 60 °C due to the high degree of adsorption. The increased temperature results in the high mobility of large dye ions, adsorbent swelling, growth of adsorbent porosity and decreased viscosity of the medium [55].

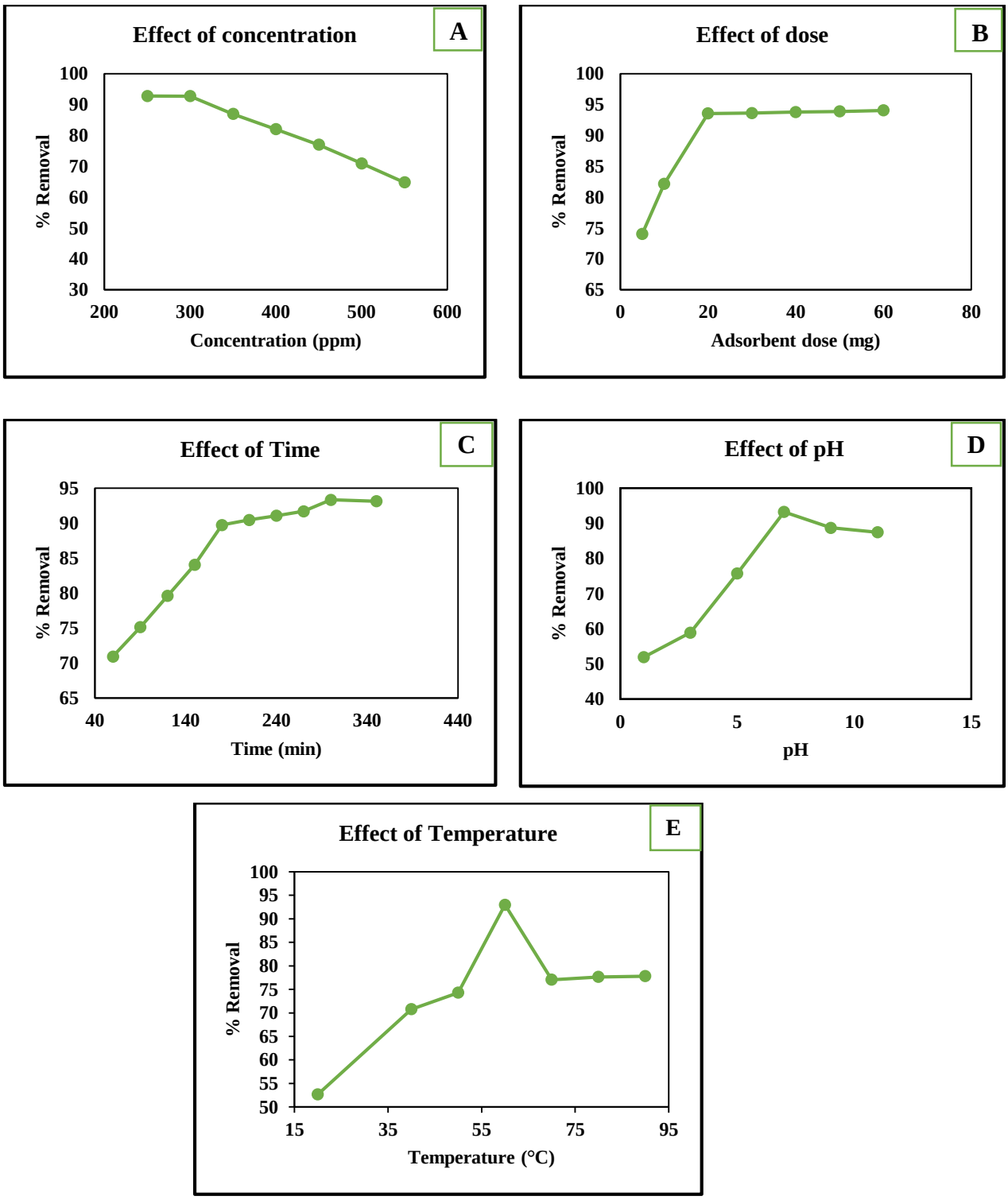

Figure 6. Adsorption graphs for different parameters (A) concentration, (B) adsorbent dose, (C) contact time, (D) pH, and (E) reaction temperature.

4.4 The non-linear isotherm models

The dye removal studies were observed by using Double Beam UV Spectrophotometer further investigating the isotherm models which have been best fitted to the experimental adsorption data. Different isotherm models were drawn which were used to describe the adsorption pathway. In order to check the interfacial phenomena between solid-liquid adsorption; different parameter-based isotherm models like Langmuir, Freundlich, D-R, Temkin, Jovanovic, Jossens, Khan and other models were studied. As from the batch study of influence of initial concentration has been observed that with the increase in concentration from lower to higher range, the

percentage removal of dye gets decreases. This behaviour in adsorption process was noticed due to the availability and unavailability of vacant sites on the Hydrogel surface. The availability of dye molecules was increasing by the gradual increase of concentration which may lead to the fulfilment of adsorbed sites and hence results in low percentage removal [56]. The non-linear two parameter-based isotherm models fitted to the experimental data are shown in Figure 7a. The non-linear form of Langmuir isotherm model as shown in Figure 7a denoting the adsorption held is a monolayer adsorption having a specific number of vacant sites onto the homogeneous surface of the adsorbent [57]. Whereas the Freundlich isotherm model describes about the multilayer adsorption of dye molecules onto the heterogeneous surface of adsorbent [58]. Similarly, the Temkin isotherm model was used to represent the indirect interactions between dye molecules and hydrogel material which depends on the linear proportionality of increasing surface coverage with decreasing heat of adsorption involving in the heterogeneous system [59, 60]. Dubinin-Radushkevich (D-R) isotherm model does not assume the surface of adsorbent to be homogeneous and gives information about the process behind adsorption either physisorption or chemisorption [60, 61]. Extending the isotherm models, the Jovanovic isotherm model is two-parameter based model which is a refined form of Langmuir model having more accuracy towards the contacting potentials while adsorption process [62].

The non-linear three parameter-based isotherm models are shown in Figure 7b. Koble Corrigan model integrates both Langmuir and Freundlich isotherms, effectively encapsulating adsorption experimental data to the equilibrium stage [46]. Redlich Peterson isotherm model was derived from the blended mode of both Langmuir and Freundlich isotherm models. According to this model, the adsorption process is not ideally related to a monolayer adsorption mechanism [63, 64]. As considering the versatility of this model, it could be applied for both homogeneous and heterogeneous systems [65]. Liu isotherm model integrates both Langmuir and Freundlich models which states that the adsorption occurs in a multilayer form having different energies onto the active sites of hydrogel material [66]. Khan isotherm model represents the adsorption of dye molecules from waste water in a multicomponent system [67]. Jossens isotherm explains about the heterogeneous surface adsorption for dye molecules [68].

The non-linear four parameter-based Fritz-Schlunder adsorption isotherm model suits for the complex multilayer adsorption onto a heterogeneous surface [69]. The Fritz-Schlunder model is shown in Figure 7c and is best fitted statistical model with the experimental data of MB dye adsorption. The parameter values for all the isotherm models are evaluated and shown in Table 2.

From Table 2; it may be concluded that the models fitted best to the experimental data and supports pathways involved in the adsorption of MB dye molecules on to the Hydrogel surface are Langmuir, Koble-Corrigan, Redlich-Peterson, Liu, Khan, Jossens and FritzSchlunder adsorption isotherm models. The results according to the R2 values indicates a combination of monolayer and multilayer adsorption process and found to be versatile towards a wide range of concentration in a homogeneous as well as in heterogeneous systems [70].

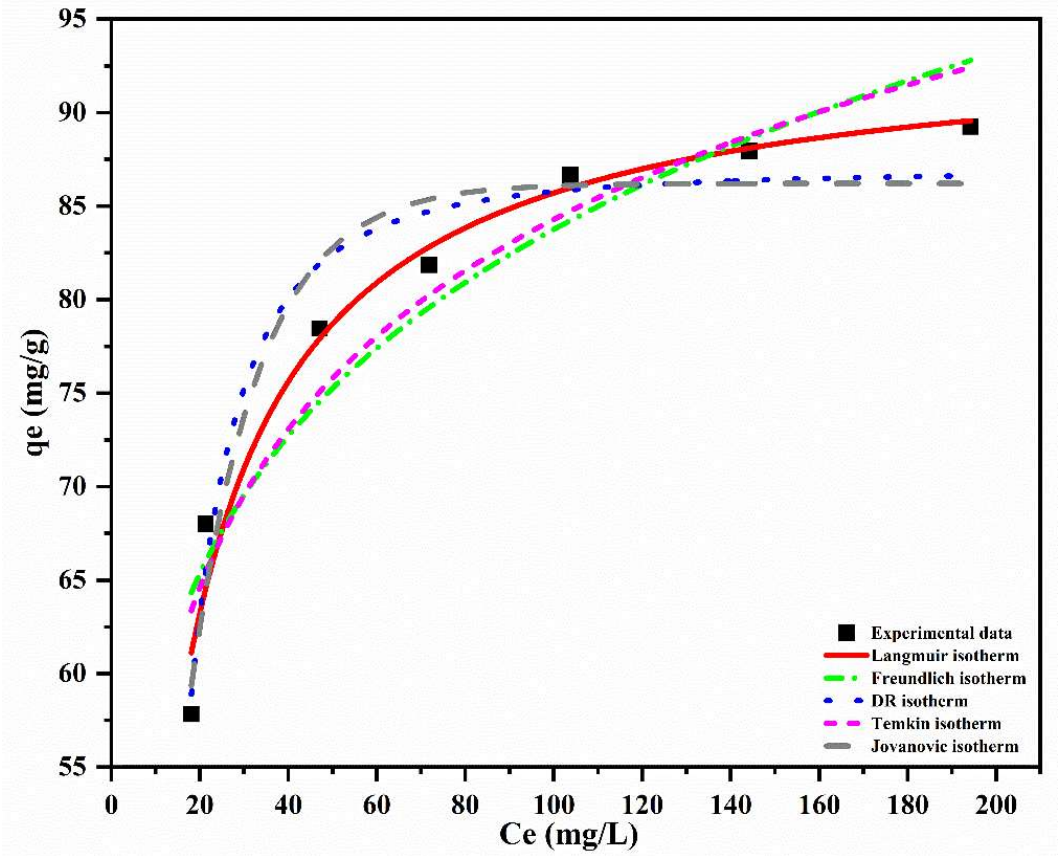

Figure 7a. Non-linear two parameter-based adsorption isotherm models.

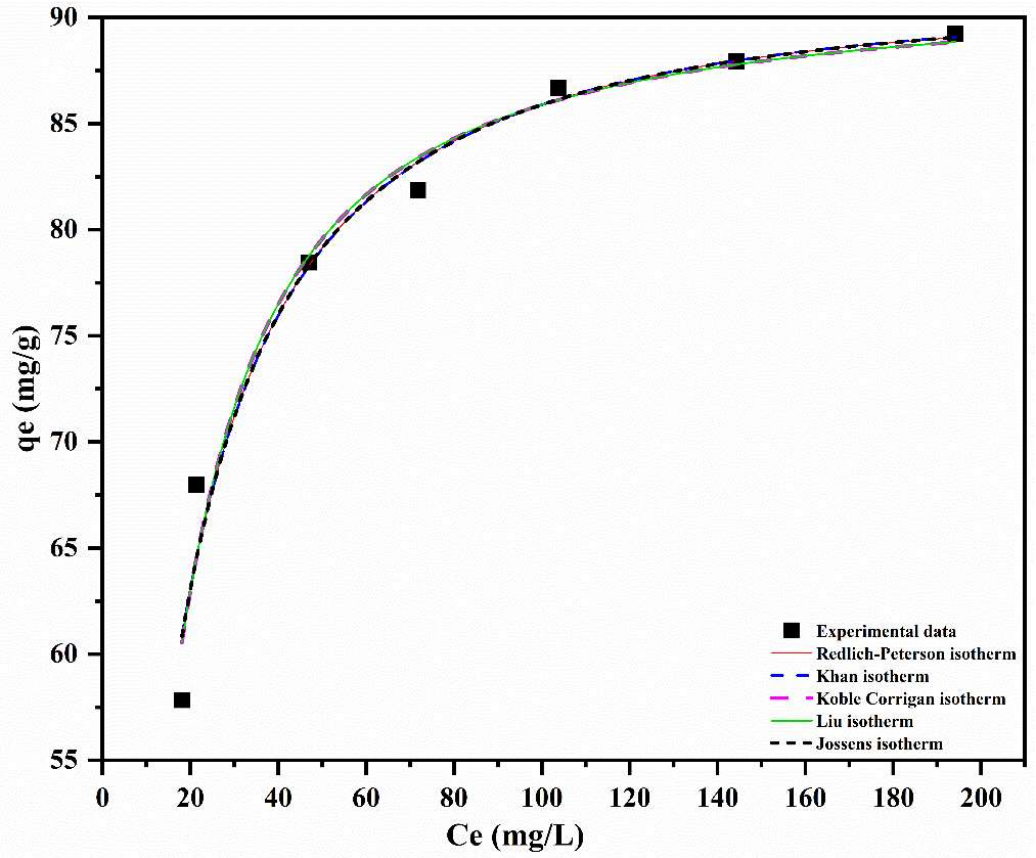

Figure 7b. Non-linear three parameter-based adsorption isotherm models.

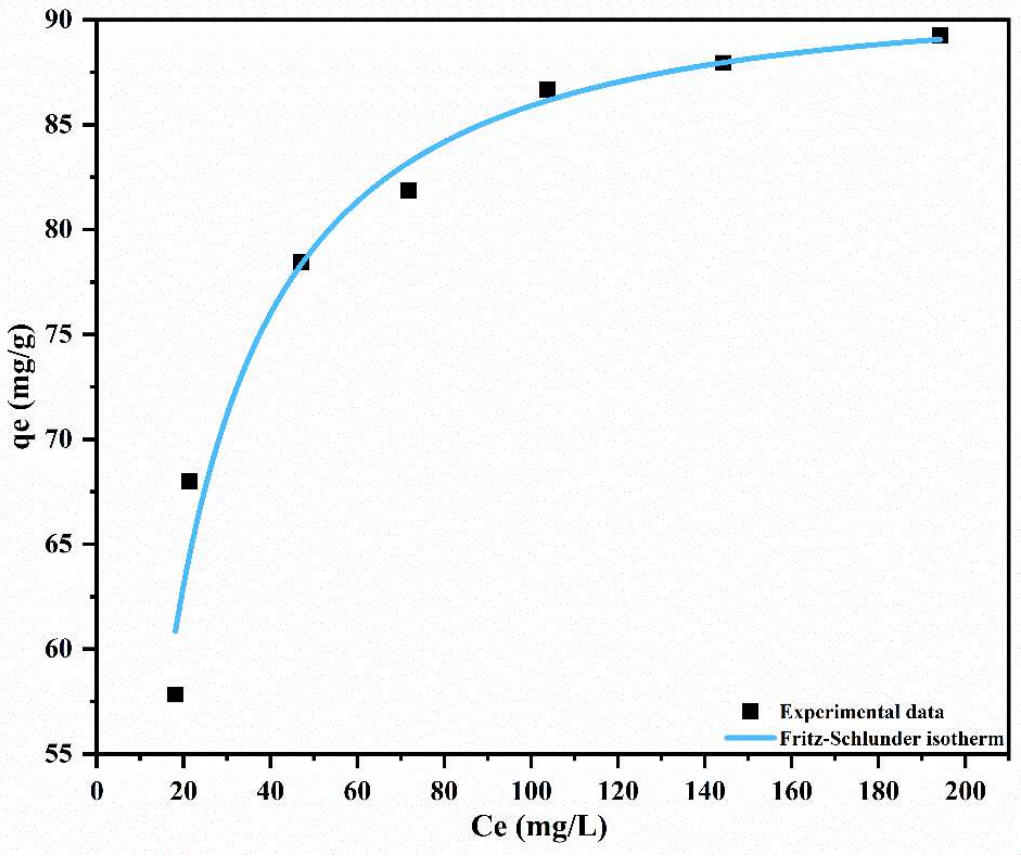

Figure 7c. Non-linear four parameter-based adsorption isotherm models.

Table 2: Parameters for non-linearized form of adsorption isotherm models.

Sr. No.	Isotherm models	Isotherm parameter	Non-linear fitting values
1.	Langmuir	q_m	94.0653
		K_L	0.1025
		R^2	**0.9702**
2.	Freundlich	n	0.1542
		K_F	41.1550
		R^2	0.8956
3.	D-R	q_m	86.9352
		β	134.5188
		R^2	0.9546
4.	Temkin	K_T	9.7885
		B	12.2402
		R^2	0.9195
5.	Jovanovic	q_m	86.2138
		K_{JV}	0.0644
		R^2	0.9354
6.	Koble Corrigan	A	5.3659

		B	0.0587
		n	1.2120
		R^2	**0.9724**
7.	Redlich Peterson	A_{RP}	0.0846
		K_{RP}	8.8113
		n	1.0194
		R^2	**0.9711**
8.	Liu	q_m	91.4083
		K_{Liu}	0.0964
		n	1.2111
		R^2	**0.9724**
9.	Khan	q_m	100.2505
		K_{KH}	0.0901
		α_{KH}	1.0214
		R^2	**0.9710**
10	Jossens	K_J	8.8113
		J_S	0.0846
		a	1.0194
		R^2	**0.9711**
11	Fritz-Schulnder	q_m	2.9684
		K_1	2.9684
		K_2	0.0846
		m	1.0194
		R^2	**0.9711**

4.5 The non-linear adsorption kinetic models

The adsorption kinetics were checked for the efficient removal of MB dye. These are most important while examining the adsorption experiment as they provide valuable information for the mechanisms and reaction pathways. The kinetic models Pseudo-first order (PFO), Pseudo-second order (PSO), Intraparticle diffusion (IPD), and Elovich models were

illustrated on the basis of R2 obtained from the best fitted model with experimental data. A brief description of all kinetic parameters and model equations is shown in Table 3. The adsorption kinetic model results are illustrated in Table 4. The experimental values were suitably fitted with PSO and Elovich kinetic models indicating that the overall rate of adsorption of MB dye molecules onto the Hydrogel surface was controlled by pseudo-second order reaction which correlates to the chemisorption phenomenon during adsorption where the adsorption rate relies on the available active sites and forming covalent bonds between adsorbent and adsorbate molecules [71]. The Elovich models indicates that there is a rapid increase in the initial adsorption rate and then

observed a gradual decrease in the adsorption rate which shows resemblance with the chemisorption phenomenon in heterogeneous systems [72, 73]. The non-linear kinetic models are shown in Figure 8.

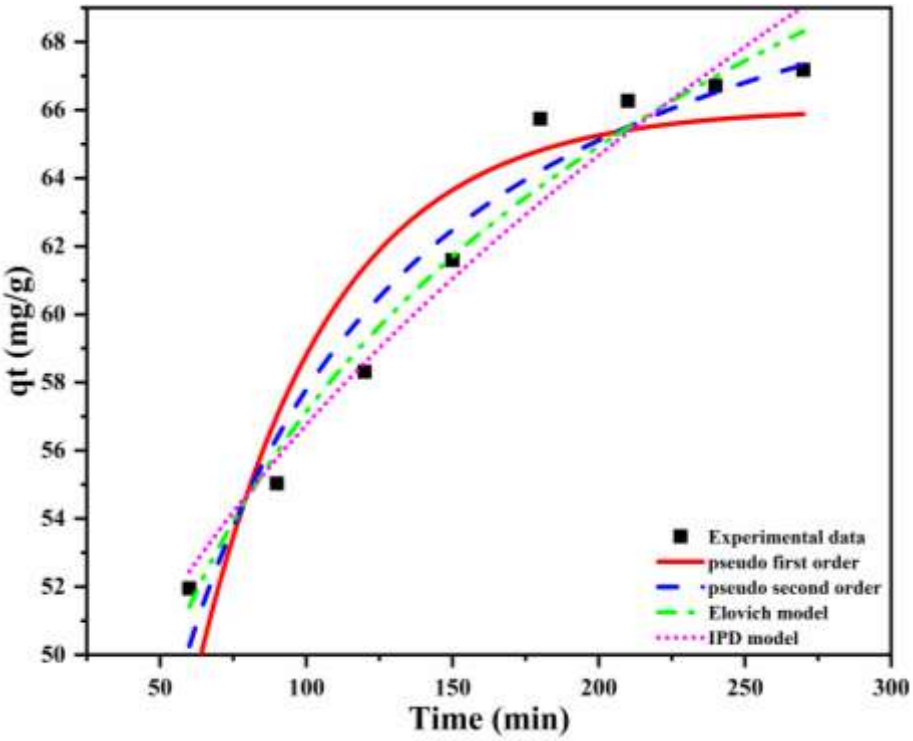

Figure 8. Non-linear adsorption kinetic models.

Table 3. Adsorption kinetic models with their non-linear forms.

Sr. No.	Kinetic models	Parameter illustration	Non-linear form equations
1.	Pseudo First Order	**q_e** is the adsorbed amount of dye at equilibrium; **q_t** is the amount of dye adsorbed at time t; **K_1** is pseudo-first order rate constant.	$q_t = q_e(1 - e^{-}K_1 t)$
2.	Pseudo Second Order	**q_e** is the adsorbed amount of dye at equilibrium; **q_t** is the amount of dye adsorbed at time t; **K_2** stands for the second order rate constant of adsorption.	$q_t = \frac{qe^2 K_2 t}{1 + K_2 q_e t}$
3.	Elovich	**α** is for the initial rate of adsorption; **β** is the activation energy of chemisorption and surface coverage.	$q_t = \frac{1}{B(\ln(\alpha\beta t + 1))}$
4.	Intraparticle Diffusion	**k_{diff}** is the intraparticle diffusion rate constant; **C** is the thickness of the boundary layer of adsorbent.	$q_t = K_{diff}\sqrt{t} + C$

Table 4. Parameter results of non-linearized form of adsorption kinetic models.

Sr. No.	Kinetic models	Kinetic parameter	Non-linear fitting values
1.	Pseudo first order	q_e	66.0483
		K_1	0.0221
		R^2	0.8612
2.	Pseudo-second order	q_e	74.5590
		K_2	4.6238
		R^2	**0.9529**
3.	Elovich	α	17.6442
		β	0.0885
		R^2	**0.9675**
4.	Intraparticle Diffusion	K_{diff}	1.9107
		C	37.6503
		R^2	0.9512

CONCLUSION

The biopolymers tragacanth gum (TG) and thiolated *Cassia fistula* (TCF) gum and polyethylene glycol (PEG) were blended and cross-linked with glutaraldehyde to form a three-dimensional hydrogel network. The synergistic effect of polymer blending and chemical cross-linking facilitated the development of a mechanically stable hydrogel network with enhanced hydrophilicity, resulting in superior swelling performance and water-retention characteristics. The hydrogel effectively removes the toxic cationic dye methylene blue and shows a maximum dye removal of 93.17 %. The synthesized hydrogel exhibited satisfactory thermal stability, which is consistent with the thermal behavior of its constituent components. Owing to this stability, the developed hydrogel shows significant potential for application in wastewater treatment. Overall, such blended hydrogel systems represent a promising class of materials for future research and technological advancements in environmental remediation.

Funding

This work was supported by the UP-CST, Lucknow (project ID. 1633; Sanction year: 2022).

Declaration of Competing Interest

The authors declare that they have no known competing financial interests or personal relationships that could have appeared to influence the work reported in this paper.

Authors contribution declaration

Jyoti Pandey: Supervision, Conceptualization, Original draft writing-review & editing, Project administration

Ruchi Singh: Methodology, Investigation, Formal analysis, Validation and Data curation, Original draft writing

Acknowledgements

RS thanks UGC for scholarship.

We acknowledge the use of ChatGPT (https://chat.openai.com/) to refine the academic language of the paper.

REFERENCES

1) Mouhamadou, S., Fryda, L., Dalhatou, S., Kaetzl, K., Talami, B., Bouza, M. O., Djakba, R., Casimir, N.H., Massai, H., & Kane, A. (2026). Adsorption performance optimisation by classical and response surface methodology towards removal of dye binary system using biowaste biochar: Kinetics, isotherms, thermodynamics and mechanistic study. *Journal of Water Process Engineering*, *86*, 109947. https://doi.org/10.1016/j.jwpe.2026.109947

2) Chang, Z., Chen, Y., Tang, S., Yang, J., Chen, Y., Chen, S., Li, P., & Yang, Z. (2020). Construction of chitosan/polyacrylate/graphene oxide composite physical hydrogel by semi-dissolution/acidification/sol-gel transition method and its simultaneous cationic and anionic dye adsorption properties. *Carbohydrate polymers*, *229*, 115431. https://doi.org/10.1016/j.carbpol.2019.115431.

3) Ali, A., Ejaz, N., Nasreen, S., Nasir, A., Qureshi, L. A., & Al-Sakkaf, B. M. (2019). Enhanced degradation of dyes present in textile effluent by ultrasound assisted electrochemical reactor. *Civil Engineering Journal*, *5*(10), 2131-2142. https://doi.org/ 10.28991/cej-2019-03091399.

4) Su, T., Wu, L., Zuo, G., Pan, X., Shi, M., Zhang, C., Qi, X., & Dong, W. (2020). Incorporation of dumbbell-shaped and Y-shaped cross-linkers in adjustable pullulan/polydopamine hydrogels for selective adsorption of cationic dyes. *Environmental research*, *182*, 109010. https://doi.org/10.1016/j.envres.2019.109010.

5) Lapwanit, S., Sooksimuang, T., & Trakulsujaritchok, T. (2018). Adsorptive removal of cationic methylene blue dye by kappa-carrageenan/poly (glycidyl methacrylate) hydrogel beads: preparation and characterization. *Journal of environmental chemical engineering*, *6*(5), 6221-6230. https://doi.org/10.1016/j.jece.2018.09.050

6) Jack Clifton, I. I., & Leikin, J. B. (2003). Methylene blue. *American journal of therapeutics*, *10*(4), 289-291. DOI: 10.1097/00045391-200307000-00009

7) Sharma, R., Kaith, B. S., Kalia, S., Pathania, D., Kumar, A., Sharma, N., Street, R.M., & Schauer, C. (2015). Biodegradable and conducting hydrogels based on Guar gum polysaccharide for antibacterial and dye removal applications. *Journal of environmental management*, *162*, 37-45. https://doi.org/10.1016/j.jenvman.2015.07.044

8) Mogharbel, A. T., & Almotiry, S. (2026). Enhanced removal of methylene blue dye via combined adsorption and photocatalytic degradation using CdS@ activated pumice stone/carrageenan composite beads. *Journal of Water Process Engineering*, *87*, 110076. https://doi.org/10.1016/j.jwpe.2026.110076

9) Molahosseini, E., Zare, H., Molaei, M., & Farahmandzadeh, F. (2025). Synthesis of Fe3O4/AC/SiO2 Magnetic Nanocomposite and Application as a High Performance, Non-Toxic, and Cost-Efficient Nanocatalyst for Removal of Methylene Blue Dye from Water. *Vacuum*, 115057. https://doi.org/10.1016/j.vacuum.2025.115057

10) Oladoye, P. O., Ajiboye, T. O., Omotola, E. O., & Oyewola, O. J. (2022). Methylene blue dye: Toxicity and potential elimination technology from wastewater. *Results in Engineering*, *16*, 100678. https://doi.org/10.1016/J.RINENG.2022.100678

11) Ghosh, D., & Bhattacharyya, K. G. (2002). Adsorption of methylene blue on kaolinite. *Applied clay science*, *20*(6), 295-300. https://doi.org/10.1016/S0169-1317(01)00081-3.

12) Sharma, S., Hasan, A., Kumar, N., & Pandey, L. M. (2018). Removal of methylene blue dye from aqueous solution using immobilized Agrobacterium fabrum biomass along with iron oxide nanoparticles as biosorbent. *Environmental Science and Pollution Research*, *25*(22), 21605-21615. https://doi.org/10.1007/s11356-018-2280-z

13) Rocha, M. A. M., Ferreira, P., Coimbra, M. A., & Nunes, C. (2020). Mechanism of iron ions sorption by chitosan-genipin films in acidic media. *Carbohydrate polymers*, *236*, 116026. https://doi.org/10.1016/j.carbpol.2020.116026.

14) Theingi, M., Tun, K. T., & Aung, N. N. (2019). Preparation, characterization and optical property of LaFeO3 nanoparticles via sol-gel combustion method. *SciMedicine Journal*, *1*(3), 151-157. https://doi.org/10.28991/SciMedJ-2019-0103-5

15) Abe, F. R., Soares, A. M., de Oliveira, D. P., & Gravato, C. (2018). Toxicity of dyes to zebrafish at the biochemical level: Cellular energy allocation and neurotoxicity. *Environmental pollution*, *235*, 255-262. https://doi.org/10.1016/j.envpol.2017.12.020

16) Xue, S., Wu, C., Pu, S., Hou, Y., Tong, T., Yang, G., Qin, Z., Wang, Z., & Bao, J. (2019). Direct Z-Scheme charge transfer in heterostructured MoO3/g-C3N4 photocatalysts and the generation of active radicals in photocatalytic dye degradations. *Environmental pollution*, *250*, 338-345. https://doi.org/10.1016/j.envpol.2019.04.010

17) Suopajärvi, T., Liimatainen, H., Hormi, O., & Niinimäki, J. (2013). Coagulation–flocculation treatment of municipal wastewater based on anionized nanocelluloses. *Chemical Engineering Journal*, *231*, 59-67. https://doi.org/10.1016/j.cej.2013.07.010

18) Wang, L., Liang, W., Yu, J., Liang, Z., Ruan, L., & Zhang, Y. (2013). Flocculation of Microcystis aeruginosa using modified larch tannin. *Environmental science & technology*, *47*(11), 5771-5777. https://doi.org/10.1021/es400793x

19) Sharma, D., Kumar, V., & Sharma, P. (2022). Synthesis, characterization and evaluation of amphoteric galactomannan derivative for the mitigation of malachite green and congo red dye from aqueous solution. *Cellulose*, *29*(2), 1035-1053. https://doi.org/10.1007/s10570-021-04332-5

20) Ahmad, T., Manzar, M. S., Georgin, J., Franco, D. S., Khan, S., Meili, L., & Ullah, N. (2023). Development of a new hyper crosslinked resin based on polyamine-isocyanurate for the efficient removal

of endocrine disruptor bisphenol-A from water. *Journal of Water Process Engineering*, *53*, 103623. https://doi.org/10.1016/j.jwpe.2023.103623

21) Li, B., Ma, J., Zhou, L., & Qiu, Y. (2017). Magnetic microsphere to remove tetracycline from water: adsorption, H2O2 oxidation and regeneration. *Chemical Engineering Journal*, *330*, 191-201. https://doi.org/10.1016/j.cej.2017.07.054

22) Shi, X., Wang, W., & Wang, A. (2011). Synthesis and enhanced swelling properties of a guar gum-based superabsorbent composite by the simultaneous introduction of styrene and attapulgite. *Journal of Polymer Research*, *18*(6), 1705-1713.
https://doi.org/10.1007/s10965-011-9576-8

23) Peppas, N. A., Huang, Y., Torres-Lugo, M., Ward, J. H., & Zhang, J. (2000). Physicochemical foundations and structural design of hydrogels in medicine and biology. *Annual review of biomedical engineering*, *2*(1), 9-29. https://doi.org/10.1146/annurev.bioeng.2.1.9

24) Zhang, L. M., Wang, G. H., Lu, H. W., Yang, C., & Yan, L. (2005). A new class of starch-based hydrogels incorporating acrylamide and vinyl pyrrolidone: effects of reaction variables on water sorption behavior. *Journal of bioactive and compatible polymers*, *20*(5), 491-501. https://doi.org/10.1177/0883911505055163

25) Maiti, S., Khillar, P. S., Mishra, D., Nambiraj, N. A., & Jaiswal, A. K. (2021). Physical and self–crosslinking mechanism and characterization of chitosan-gelatin-oxidized guar gum hydrogel. *Polymer Testing*, *97*, 107155.
https://doi.org/10.1016/j.polymertesting.2021.107155

26) Nath, J., Kumar, S., & Kumar, V. (2023). Response surface methodology-based modeling and optimization of fenugreek gum-based hydrogel for efficient removal of malachite green dye. *Journal of Molecular Structure*, *1293*, 136234.
https://doi.org/10.1016/j.molstruc.2023.136234

27) Bhattacharya, A., & Misra, B. N. (2004). Grafting: a versatile means to modify polymers: techniques, factors and applications. *Progress in polymer science*, *29*(8), 767-814. https://doi.org/10.1016/j.progpolymsci.2004.05.002

28) Sen, G., Mishra, S., Prasad Dey, K., & Bharti, S. (2014). Synthesis, characterization and application of novel polyacrylamide-grafted barley. *Journal of Applied Polymer Science*, *131*(22). https://doi.org/10.1002/app.41046

29) Chawla, P., Ranjan Srivastava, A., Pandey, P., & Chawla, V. (2014). Hydrogels: A journey from diapers to gene delivery. *Mini Reviews in Medicinal Chemistry*, *14*(2), 154-167. https://doi.org/10.2174/1389557513666140103110243

30) Sionkowska, A. (2020). Natural polymers as components of blends for biomedical applications. In *Polymeric Biomaterials* (pp. 327-360). CRC Press. https://doi.org/10.1201/9780429142413

31) Garnica-Palafox, I., Sánchez-Arévalo, F., Velasquillo, C., García-Carvajal, Z., García-López, J., Ortega-Sánchez, C., et al. (2014). Mechanical and structural response of a hybrid hydrogel based on chitosan and

poly(vinyl alcohol) cross-linked with epichlorohydrin for potential use in tissue engineering. *Journal of Biomaterials Science, Polymer Edition*, *25*(1), 32-50. https://doi.org/10.1080/09205063.2013.833441

32) Hu, H., Xin, J. H., Hu, H., Chan, A., & He, L. (2013). Glutaraldehyde–chitosan and poly (vinyl alcohol) blends, and fluorescence of their nano-silica composite films. *Carbohydrate polymers*, *91*(1), 305-313. https://doi.org/10.1016/j.carbpol.2012.08.038

33) Garnica-Palafox, I. M., & Sánchez-Arévalo, F. M. (2016). Influence of natural and synthetic crosslinking reagents on the structural and mechanical properties of chitosan-based hybrid hydrogels. *Carbohydrate Polymers*, *151*, 1073-1081. https://doi.org/10.1016/j.carbpol.2016.06.036

34) Bispo, V. M., Mansur, A. A., Barbosa-Stancioli, E. F., & Mansur, H. S. (2010). Biocompatibility of nanostructured chitosan/poly (vinyl alcohol) blends chemically crosslinked with genipin for biomedical applications. *Journal of biomedical nanotechnology*, *6*(2), 166-175. https://doi.org/10.1166/jbn.2010.1110

35) Mallakpour, S., & Tabesh, F. (2021). Effective adsorption of methylene blue dye from water solution using renewable natural hydrogel bionanocomposite based on tragacanth gum: Linear-nonlinear calculations. *International Journal of Biological Macromolecules*, *187*, 319-324. https://doi.org/10.1016/j.ijbiomac.2021.07.105

36) Nagaraja, K., Rao, K. M., Reddy, G. V., & Rao, K. K. (2021). Tragacanth gum-based multifunctional hydrogels and green synthesis of their silver nanocomposites for drug delivery and inactivation of multidrug resistant bacteria. *International journal of biological macromolecules*, *174*, 502-511. https://doi.org/10.1016/j.ijbiomac.2021.01.203

37) Kulanthaivel, S., Agarwal, T., Rathnam, V. S., Pal, K., & Banerjee, I. (2021). Cobalt doped nano-hydroxyapatite incorporated gum tragacanth-alginate beads as angiogenic-osteogenic cell encapsulation system for mesenchymal stem cell based bone tissue engineering. *International journal of biological macromolecules*, *179*, 101-115. https://doi.org/10.1016/j.ijbiomac.2021.02.136

38) Ali, S., Anjum, M. A., Nawaz, A., Naz, S., Ejaz, S., Sardar, H., & Saddiq, B. (2020). Tragacanth gum coating modulates oxidative stress and maintains quality of harvested apricot fruits. *International Journal of Biological Macromolecules*, *163*, 2439-2447. https://doi.org/10.1016/j.ijbiomac.2020.09.179

39) Apoorva, A., Rameshbabu, A. P., Dasgupta, S., Dhara, S., & Padmavati, M. (2020). Novel pH-sensitive alginate hydrogel delivery system reinforced with gum tragacanth for intestinal targeting of nutraceuticals. *International Journal of Biological Macromolecules*, *147*, 675-687. https://doi.org/10.1016/j.ijbiomac.2020.01.027

40) Jaymand, M. (2024). Biosorptive removal of cationic dyes from ternary system using a magnetic nanocomposite hydrogel based on modified tragacanth gum. *Carbohydrate Polymer Technologies and Applications*, *7*, 100403. https://doi.org/10.1016/j.carpta.2023.100403

41) Ranjbar-Mohammadi, M., Rahimdokht, M., & Pajootan, E. (2019). Low cost hydrogels based on gum Tragacanth and TiO2 nanoparticles: characterization and RBFNN modelling of methylene blue dye

removal. *International journal of biological macromolecules*, *134*, 967-975. https://doi.org/10.1016/j.ijbiomac.2019.05.026

42) Sahraei, R., Pour, Z. S., & Ghaemy, M. (2017). Novel magnetic bio-sorbent hydrogel beads based on modified gum tragacanth/graphene oxide: Removal of heavy metals and dyes from water. *Journal of cleaner production*, *142*, 2973-2984. https://doi.org/10.1016/j.jclepro.2016.10.170

43) Mallakpour, S., & Tabesh, F. (2021). Green and plant-based adsorbent from tragacanth gum and carboxyl-functionalized carbon nanotube hydrogel bionanocomposite for the super removal of methylene blue dye. *International journal of biological macromolecules*, *166*, 722-729. https://doi.org/10.1016/j.ijbiomac.2020.10.229

44) Pandey, J., Singh, B. D., Khanam, H., Tiwari, B., Azaz, T., & Singh, R. (2024). Cassia fistula galactomannan stabilized copper nanocatalyst as an efficient, recyclable heterogeneous catalyst for the fast clickable [3+ 2] Huisgen cycloadditions in water. *International Journal of Biological Macromolecules*, *255*, 128098. https://doi.org/10.1016/j.ijbiomac.2023.128098

45) Thombre, N. A., Pawar, K. N., Patil, Y. A., & Kshirsagar, S. J. (2018). Novel thiolated Ceasalpinia Pulcherrima: Synthesis, characterization and evaluation as mucoadhesive in situ gelling agent. *Pharmaceutical Journal of Sri Lanka*, *8*(1). https://doi.org/10.4038/pjsl.v8i1.23

46) Alkurdi, S. S., Al-Juboori, R. A., Bundschuh, J., Bowtell, L., & Marchuk, A. (2021). Inorganic arsenic species removal from water using bone char: A detailed study on adsorption kinetic and isotherm models using error functions analysis. *Journal of Hazardous Materials*, *405*, 124112, 1-14. https://doi.org/10.1016/j.jhazmat.2020.124112

47) Nabil, G. M., Althomali, R. H., & Elsyed, M. (2026). Novel sustainable and recyclable nanobiosorbent of cross-lined zeolite with nanobiochar and cellulose for the effecious alleviation of lead (II) from wastewater. *International Journal of Biological Macromolecules*, 151440. https://doi.org/10.1016/j.ijbiomac.2026.151440

48) Lee, C. G., Alvarez, P. J., Nam, A., Park, S. J., Do, T., Choi, U. S., & Lee, S. H. (2017). Arsenic (V) removal using an amine-doped acrylic ion exchange fiber: kinetic, equilibrium, and regeneration studies. *Journal of Hazardous Materials*, *325*, 223-229. https://doi.org/10.1016/j.jhazmat.2016.12.003

49) Dicharry, R. M., Ye, P., Saha, G., Waxman, E., Asandei, A. D., & Parnas, R. S. (2006). Wheat Gluten−Thiolated poly (vinyl alcohol) blends with improved mechanical properties. *Biomacromolecules*, *7*(10), 2837-2844. https://doi.org/10.1021/bm060432n

50) Bernkop-Schnurch, A., Hornof, M. & Zoidl, T. (2003). Thiolated polymers-thiomers: Synthesis and *in vitro* evaluation of chitosan-2-iminothiolane conjugates. *International Journal of Pharmaceutics*, 260, 229-237. https://doi.org/10.1016/S0378-5173(03)00271-0

51) Falade, K. O., & Okafor, C. A. (2015). Physical, functional, and pasting properties of flours from corms of two Cocoyam (Colocasia esculenta and Xanthosoma sagittifolium) cultivars. *Journal of Food Science and Technology*, *52*(6), 3440-3448. https://doi.org/10.1007/s13197-014-1368-9

52) Nagpal, M., Aggarwal, G., Jain, K. U., & Madan, J. (2017). Extraction of gum from *Abelmoschus esculentus* physicochemical peculiarity and antioxidant prepatent. *Asian J. Pharm. Clin. Res.*, 10, 174-179. http://dx.doi.org/10.22159/ajpcr.2017.v10i9.19260

53) Shah, R. B., Tawakkul, M. A., & Khan, M. A. (2008). Comparative evaluation of flow for pharmaceutical powders and granules. *Aaps Pharmscitech*, *9*(1), 250-258. https://doi.org/10.1208/s12249-008-9046-8

54) Grewal, P., Mundlia, J., & Ahuja, M. (2019). Thiol modified Moringa gum–A potential bioadhesive polymer. *Carbohydrate polymers*, *209*, 400-408. https://doi.org/10.1016/j.carbpol.2018.12.100

55) Irfan, M., ul Hasan, I. M., Jafir, M., Li, C., Hu, J., ud Din, M. M., Hussain, K., Zhu, Y., & Zheng, L. (2026). Removal of arsenic from aqueous solution using a surface-functionalized magnetic biochar derived from Chlorella. *Marine Pollution Bulletin*, *227*, 119440. https://doi.org/10.1016/j.marpolbul.2026.119440

56) Zhang, X., Wu, S., Liu, Y., Wang, Z., Zhang, H., & Xiao, R. (2023). Removal of Cr (VI) from aqueous solution by Rice-husk-based activated carbon prepared by Dual-mode heating method. *Carbon Resources Conversion*, *6*(2), 76-84.
https://doi.org/10.1016/j.crcon.2023.01.003

57) Langmuir, I. (1918). The adsorption of gases on plane surfaces of glass, mica and platinum. *Journal of the American Chemical society*, *40*(9), 1361-1403.
https://doi.org/10.1021/ja02242a004

58) Kundu, S., & Gupta, A. K. (2006). Arsenic adsorption onto iron oxide-coated cement (IOCC): regression analysis of equilibrium data with several isotherm models and their optimization. *Chemical Engineering Journal*, *122*(1-2), 93-106.
https://doi.org/10.1016/j.cej.2006.06.002

59) Musah, M., Azeh, Y., Mathew, J. T., Umar, M. T., Abdulhamid, Z., & Muhammad, A. I. (2022). Adsorption kinetics and isotherm models: a review. *Caliphate Journal of Science & Technology*, *4*(1), 20-26. https://dx.doi.org/10.4314/cajost.v4i1.3

60) Chen, X., Hossain, M. F., Duan, C., Lu, J., Tsang, Y. F., Islam, M. S., & Zhou, Y. (2022). Isotherm models for adsorption of heavy metals from water-A review. *Chemosphere*, *307*, 135545, 1-14. https://doi.org/10.1016/j.chemosphere.2022.135545

61) Neisan, R. S., Saady, N. M. C., Bazan, C., & Zendehboudi, S. (2025). Optimization of arsenic removal from water using novel renewable adsorbents derived from orange peels. *Waste Management Bulletin*, *3*(2), 21-35. https://doi.org/10.1016/j.wmb.2025.02.006

62) Tanko, D. B., Ahulle, W. R., Chahul, H. F., & Saviour, I. M. (2026). Review of adsorption isotherms models. *Applied Water Science*. https://doi.org/10.1007/s13201-025-02682-0

63) Juturu, R., Murty, V. R., & Selvaraj, R. (2024). Efficient adsorption of Cr (VI) onto hematite nanoparticles: ANN, ANFIS modelling, isotherm, kinetic, thermodynamic studies and mechanistic insights. *Chemosphere*, *349*, 140731.
https://doi.org/10.1016/j.chemosphere.2023.140731

64) Nabil, G. M., Althomali, R. H., & Mahmoud, M. E. (2025). Pioneering nanobiosorbent of doped cellulose-gelatin hydrogel into carbon quantum dots and magnesium ferrite for effective removal of Cr (VI). *International Journal of Biological Macromolecules*, 147119. https://doi.org/10.1016/j.ijbiomac.2025.147119

65) Zhao, D., Yu, Y., & Chen, J. P. (2016). Fabrication and testing of zirconium-based nanoparticle-doped activated carbon fiber for enhanced arsenic removal in water. *RSC Advances*, *6*(32), 27020-27030. https://doi.org/10.1039/C5RA25030G

66) Grimm, A., Conrad, S., Gentili, F. G., Mikkola, J. P., Hu, T., Lassi, U., Silva, L.F.O., Lima, E.C., & dos Reis, G. S. (2025). Highly efficient boron/sulfur-modified activated biochar for removal of reactive dyes from water: Kinetics, isotherms, thermodynamics, and regeneration studies. *Colloids and Surfaces A: Physicochemical and Engineering Aspects*, *713*, 136486. https://doi.org/10.1016/j.colsurfa.2025.136486

67) Yusif, S. Y., & Golabiazar, R. (2025). Efficient photocatalytic degradation of emerging contaminants using novel metal-organic frameworks: investigation of linear and nonlinear kinetics, isotherm models, and thermodynamics. *Journal of Water Process Engineering*, *74*, 107772. https://doi.org/10.1016/j.jwpe.2025.107772

68) Albishri, A. K., Alqarni, S. A., Alharbi, M. M., Khashoqji, M. M., Alatawi, R., Alkhamis, K. M., Keshk, A.A., & El-Metwaly, N. M. (2026). Electrospun chitosan/PEI/PVDF nanofiber membrane for fluoride removal: Interfacial adsorption mechanism, structure–property relationships, thermodynamics, and process optimization. *Colloids and Surfaces A: Physicochemical and Engineering Aspects*, *736*, 139667. https://doi.org/10.1016/j.colsurfa.2026.139667

69) Ashraf, E. H., Amer, H., Edbey, K., & Bhattarai, A. (2025). Xanthated Arbutus Pavarii leaves as a novel biosorbent for methyl violet 6b: A comparative nonlinear regression approach for kinetic isotherm, and thermodynamic modeling. *Results in Chemistry*, 102976. https://doi.org/10.1016/j.rechem.2025.102976

70) Koble, R. A., & Corrigan, T. E. (1952). Adsorption isotherms for pure hydrocarbons. *Industrial & Engineering Chemistry*, *44*(2), 383-387.
https://doi.org/10.1021/ie50506a049

71) Kim, E. J., Lee, C. S., Chang, Y. Y., & Chang, Y. S. (2013). Hierarchically structured manganese oxide-coated magnetic nanocomposites for the efficient removal of heavy metal ions from aqueous systems. *ACS applied materials & interfaces*, *5*(19), 9628-9634. https://doi.org/10.1021/am402615m

72) Khan, M. I., Sutanto, M. H., Napiah, M. B., Zahid, M., & Usman, A. (2020, May). Optimization of cementitious grouts for semi-flexible pavement surfaces using response surface methodology. In *IOP Conference Series. Earth and Environmental Science* (Vol. 498, No. 1). IOP Publishing. doi:10.1088/1755-1315/498/1/012004

73) Helmi, M., Tahvildari, K., Hemmati, A., Azar, P. A., & Safekordi, A. (2022). Converting waste cooking oil into biodiesel using phosphomolybdic acid/clinoptilolite as an innovative green catalyst via electrolysis procedure; optimization by response surface methodology (RSM). *Fuel Processing Technology*, *225*, 107062. https://doi.org/10.1016/j.fuproc.2021.107062